# Inferring the anthropogenic $NO_x$ emission trend over the United States during 2003 - 2017 from satellite observations: Was there a flattening of the emission trend after the Great Recession?

Jianfeng Li[1, a], Yuhang Wang[1*]

[1] School of Earth and Atmospheric Sciences, Georgia Institute of Technology, Atlanta, Georgia, USA

[a] Now at Pacific Northwest National Laboratory, Richland, WA, USA

[*] *Correspondence to* Yuhang Wang (yuhang.wang@eas.gatech.edu)

# Abstract

We illustrate the nonlinear relationships among anthropogenic $NO_x$ emissions, $NO_2$ tropospheric vertical column densities (TVCDs), and $NO_2$ surface concentrations using model simulations for July 2011 over the contiguous United States (CONUS). The variations of $NO_2$ surface concentrations and TVCDs are generally consistent and reflect well anthropogenic $NO_x$ emission variations for high-anthropogenic-$NO_x$ emission regions. For low-anthropogenic-$NO_x$ emission regions, however, nonlinearity in the anthropogenic emission-TVCD relationship due to emissions from lightning and soils, chemistry, and physical processes makes it difficult to use satellite observations to infer anthropogenic $NO_x$ emission changes. The analysis is extended to 2003 – 2017. Similar variations of $NO_2$ surface measurements and coincident satellite $NO_2$ TVCDs over urban regions are in sharp contrast to the large variation differences between surface and satellite observations over rural regions. We find a continuous decrease of anthropogenic $NO_x$ emissions after 2011 by examining surface and satellite measurements in CONUS urban regions, but the decreasing rate is lower by 9% - 46% than the pre-2011 period.

# 1. Introduction

Anthropogenic emissions of nitrogen oxides ($NO_x = NO_2 + NO$) adversely affect the environment, not only because of their direct detrimental impacts on human health (Greenberg et al., 2016; Greenberg et al., 2017; Heinrich et al., 2013; Weinmayr et al., 2009), but also their fundamental roles in the formation of ozone, acid rain, and fine particles, all of which have negative environmental impacts (Crouse et al., 2015; Kampa and Castanas, 2008; Myhre et al., 2013; Pandey et al., 2005; Singh and Agrawal, 2007). About 48.8 Tg N $yr^{-1}$ of $NO_x$ are emitted globally from both anthropogenic (77%) and natural (23%) sources, such as fossil fuel combustion, biomass and biofuel burning, soil bacteria, and lightning (Seinfeld and Pandis, 2016). 3.85 Tg N, 0.24 Tg N, and 0.66 Tg N of anthropogenic, soil, and lightning $NO_x$, respectively, were emitted from the U.S. in 2014 on the basis of the 2014 National Emission Inventory (NEI2014) and the GEOS-Chem model simulations (Silvern et al., 2019); vehicle sources and fuel combustions accounted for 93% of the total anthropogenic $NO_x$ emissions (EPA, 2017).

The U.S. anthropogenic $NO_x$ emissions during the 2010s declined dramatically compared to the mid-2000s (EPA, 2018; Xing et al., 2013) due to stricter air quality regulations and emission control technology improvements, such as the phase-in of Tier II vehicles during 2004 – 2009 and the switch of power plants from coal to natural gas (De Gouw et al., 2014; McDonald et al., 2018). The overall reduction (about 30% - 50%) of anthropogenic $NO_x$ emissions from the mid-2000s to the 2010s was corroborated by observed decreasing of vehicle $NO_x$ emission factors, $NO_2$ surface concentrations, nitrate wet deposition flux (Figure S1), and $NO_2$ tropospheric vertical column densities (TVCDs) (Bishop and Stedman, 2015; Georgoulias et al., 2019; Li et al., 2018; McDonald et al., 2018; Miyazaki et al., 2017; Russell et al., 2012; Tong et al., 2015). However, the detailed $NO_x$ emission changes after the Great Recession (from December 2007 to

June 2009) are highly uncertain. On the one hand, the U.S. Environmental Protection Agency (EPA) estimated that the Great Recession had a slight impact on the anthropogenic $NO_x$ emission trend, and the anthropogenic $NO_x$ emissions decreased steadily from 2002 to 2017 (Figure S2), although the emission decrease rate slowed down by about 20% after 2010 (-5.8% $yr^{-1}$ for 2002 – 2010, and -4.7% $yr^{-1}$ for 2010 – 2017, Table 1) (EPA, 2018). Fuel-based emission estimates in Los Angeles also showed a steady decrease of anthropogenic $NO_x$ emissions after 2000 and a small impact of the Great Recession on anthropogenic $NO_x$ emission decrease trend (Hassler et al., 2016). The continuous decrease of anthropogenic $NO_x$ emissions was consistent with the ongoing reduction of vehicle emissions (McDonald et al., 2018). On the other hand, Miyazaki et al. (2017) and Jiang et al. (2018) found that the U.S. $NO_x$ emissions derived from satellite $NO_2$ TVCDs, including OMI (the Ozone Monitoring Instrument), SCIAMACHY (SCanning Imaging Absorption SpectroMeter for Atmospheric CHartography), and GOME-2A (Global Ozone Monitoring Experiment – 2 onboard METOP-A), were almost flat from 2010 - 2015 and suggested that the decrease of $NO_x$ emissions was only significant before 2010, which was completely different from the bottom-up and fuel-based emission estimates.

A complicating factor in inferring anthropogenic $NO_x$ emission trends from the observations of $NO_2$ surface concentrations and satellite $NO_2$ TVCDs is their nonlinear dependences on anthropogenic $NO_x$ emissions (Gu et al., 2013; Gu et al., 2016; Lamsal et al., 2011). Although the decrease rates of both $NO_2$ surface concentrations and coincident OMI $NO_2$ TVCDs slowed down after the Great Recession over the United States, Tong et al. (2015), Lamsal et al. (2015) and Jiang et al. (2018) found that the slowdown of the decrease rates derived from $NO_2$ surface concentrations is 12% - 79% less than those of $NO_2$ TVCDs (Table 1). Secondly, the slowdown of the decrease rates of $NO_2$ surface concentrations and OMI TVCDs over cities and power plants (Russell et al., 2012; Tong et al., 2015) is significantly less than those over the whole contiguous United States (CONUS) (Jiang et al., 2018; Lamsal et al., 2015). Moreover, Zhang et al. (2018)

found that filtering out lightning-affected measurements could significantly improve the comparison of $NO_2$ surface concentration and OMI $NO_2$ TVCD trends over the CONUS.

In this study, we carefully investigate the relationships among anthropogenic $NO_x$ emissions, $NO_2$ surface concentrations, and $NO_2$ TVCDs over the CONUS and evaluate the impact of the relationships on inferring anthropogenic $NO_x$ emission changes and trends from surface and satellite observations. Section 2 describes the model and datasets used in this study, including the Regional chEmistry and trAnsport Model (REAM), the EPA Air Quality System (AQS) $NO_2$ surface observations, and $NO_2$ TVCD products from OMI, GOME-2A, GOME-2B (GOME2 onboard METOP-B), and SCIAMACHY. In Section 3, we examine the nonlinear relationships among anthropogenic $NO_x$ emissions, $NO_2$ surface concentrations, and $NO_2$ TVCDs using model simulations. Accounting for the effects of background sources, physical processes, and chemical nonlinearity, we then investigate the anthropogenic $NO_x$ emission trends and changes from 2003 – 2017 over the CONUS. Finally, section 4 gives a summary of the study.

# 2. Model and Data Description

## 2.1 REAM

The REAM model has been applied and evaluated in many research applications including ozone simulation and forecast, emission inversion and evaluations, and mechanistic studies of chemical and physical processes (Alkuwari et al., 2013; Cheng et al., 2017; Cheng et al., 2018; Choi et al., 2008a; Choi et al., 2008b; Gu et al., 2013; Gu et al., 2014; Koo et al., 2012; Liu et al., 2012; Liu et al., 2014; Wang et al., 2007; Yang et al., 2011; Zhang et al., 2017; Zhang et al., 2018; Zhang and Wang, 2016; Zhao and Wang, 2009; Zhao et al., 2009a; Zhao et al., 2010). REAM used in this work, the model domain of which is shown in Figure 3, has 30 vertical layers in the troposphere, and the horizontal resolution is $36 \times 36$ km$^2$. The model is driven by

meteorology fields from a Weather and Research Forecasting (WRF, version 3.6) model simulation initialized and constrained by the NCEP coupled forecast system model version 2 (CFSv2) products (Saha et al., 2011). The chemistry mechanism is based on GEOS-Chem v11.01 with updated reaction rates and aerosol uptake of isoprene nitrates (Fisher et al., 2016). Chemistry boundary conditions and initializations are from a GEOS-Chem (2° × 2.5°) simulation. Hourly anthropogenic emissions on weekdays are based on the 2011 National Emission Inventory (NEI2011), while weekend anthropogenic emissions are set to be two-thirds of the weekday emissions (Beirle et al., 2003; Choi et al., 2012). Biogenic VOC emissions are estimated using the Model of Emissions of Gases and Aerosols from Nature (MEGAN) v2.10 (Guenther et al., 2012). $NO_x$ emissions from soils are based on the Yienger and Levy (YL) scheme (Li et al., 2019; Yienger and Levy, 1995). The cloud-to-ground (CG) lightning flashes are calculated following Choi et al. (2005) and Zhao et al. (2009a) with the parameterization of CG flash rate as a function of convective mass fluxes and convective available potential energy (CAPE). The ratios of intra-cloud (IC) lightning flashes to CG flashes are parameterized as a function of the height between the freezing layer and the cloud top (Luo et al., 2017; Price and Rind, 1992). In this study, 250 moles of NO are emitted per CG or IC flash (Zhao et al., 2009a). As a result, on weekdays in July 2011, REAM has mean anthropogenic $NO_x$ emissions of $7.4 \times 10^{10}$ molecules $cm^{-2}$ $s^{-1}$, mean soil $NO_x$ emissions of $1.2 \times 10^{10}$ molecules $cm^{-2}$ $s^{-1}$, and mean lightning $NO_x$ emissions of $3.4 \times 10^{10}$ molecules $cm^{-2}$ $s^{-1}$ over the CONUS.

## 2.2 Satellite $NO_2$ TVCDs

In this study, we use $NO_2$ TVCD products from four satellite sensors in the past decade, including SCIAMACHY, GOME-2A, GOME-2B, and OMI, the spectrometers onboard sun-synchronous satellites to monitor atmospheric trace gases. The SCIAMACHY instrument onboard the Environmental Satellite (ENVISAT) has an equator overpass time of 10:00 Local time (LT) and a nadir pixel resolution of 60 × 30 $km^2$. The GOME-2 instruments on Metop-A

(named as GOME-2A) and Metop-B (GOME-2B) satellites cross the equator at 9:30 LT and have a nadir resolution of 80 × 40 $km^2$. After July 15, 2013, the nadir resolution of GOME-2A became 40 × 40 $km^2$ with a smaller scanning swath. The OMI onboard the EOS-Aura satellite has a nadir resolution of 24 × 13 $km^2$ and overpasses the equator around 13:45 LT. More detailed information about these instruments is summarized in Table S1. These instruments measure backscattered solar radiation from the atmosphere in the ultraviolet and visible wavelength. The radiation measurements in the wavelength of 402 - 465 nm are then used to retrieve $NO_2$ VCDs. The retrieval process consists of three steps: 1) converting radiation observations to $NO_2$ slant column densities (SCDs) by using the Differential Optical Absorption Spectroscopy (DOAS) spectral fitting method; 2) separating tropospheric SCDs and stratospheric SCDs from the total $NO_2$ SCDs; 3) dividing the $NO_2$ tropospheric SCDs by the tropospheric air mass factors (AMF) to compute VCDs.

The product archives we use in this study include GOME-2B (TM4NO2A v2.3), SCIAMACHY (QA4ECV v1.1), GOME-2A (QA4ECV v1.1), OMI (QA4ECV v1.1, hereafter referred to as OMI-QA4ECV), OMNO2 (SPv3, hereafter referred to as OMI-NASA), and the Berkeley High-Resolution $NO_2$ products (v3.0B, hereafter referred to as OMI-BEHR). OMI-BEHR uses the tropospheric SCDs from OMI-NASA products but updates some inputs for the tropospheric AMF calculation (Laughner et al., 2018). These product archives have been previously validated (Boersma et al., 2018; Drosoglou et al., 2017; Drosoglou et al., 2018; Krotkov et al., 2017; Laughner et al., 2018; Wang et al., 2017; Zara et al., 2018). Generally, the pixel-size uncertainties of these products are > 30% over polluted regions under clear-sky conditions. We summarize the basic information about these products in Table S2. To keep the high quality and sampling consistency of $NO_2$ TVCD datasets, we chose pixel-size $NO_2$ TVCD data using the criteria listed in Table S3. After the selection, we re-gridded the pixel-size data into the REAM 36 × 36 $km^2$ grid cells and calculate the seasonal means of each grid cell with

corresponding daily values on weekdays (winter: January, February, and December; spring: March, April, and May; summer: June, July, and Autumn; autumn: September, October, and November). We excluded weekend data in this study to minimize the impacts of weekend $NO_x$ emission reduction, leading to different $NO_2$ TVCDs between weekdays and weekends (Figure S3).

Satellite TVCD measurements can show large variations and apparent discontinuities due in part to the effects of cloud, lightning $NO_x$, the shift of satellite pixel coverage, and retrieval uncertainties (Figure S3; e.g., (Boersma et al., 2018; Zhang et al., 2018)). However, continuous and consistent measurements are required for reliable trend analyses. In addition to the criteria of data selection in Table S3, we compute the seasonal relative 90$^{th}$ percentile confidence interval, defined as RCI = (X(95$^{th}$ percentile) - X(5$^{th}$ percentile)) / mean(X), where X is the daily $NO_2$ TVCD for a given season. To compute the seasonal trend, we require that RCI is < 50% for the selected season every year in the analysis period (Table S3). About 45% of data are removed as a result.

## 2.3 Surface $NO_2$ measurements

Hourly surface $NO_2$ measurements from 2003 - 2017 are from the EPA AQS monitoring network (archived on https://www.epa.gov/outdoor-air-quality-data). Most AQS monitoring sites use the Federal Reference Method (FRM) — gas-phase chemiluminescence to measure $NO_2$. Few sites use the Federal Equivalent Method (FEM) – photolytic-chemiluminescence or the Cavity Attenuated Phase Shift Spectroscopy (CAPS) method. FRM and FEM are indirect methods, in which $NO_2$ is first converted to NO and then NO is measured through chemiluminescence measurement of $NO_2$* produced by NO + $O_3$. The difference is that FRM uses heated reducers/catalysts for the conversion of $NO_2$ to NO and FEM uses photolysis of $NO_2$ to NO. The conversion to NO in the FRM instruments is not specific to $NO_2$, and non-$NO_x$ active nitrogen

compounds ($NO_z$) can also be reduced by the catalysts, which would cause high biases of $NO_2$ measurements, while the FEM method is sensitive to the photolysis conversion efficiency of $NO_2$ to NO (Beaver et al., 2012; Beaver et al., 2013; Lamsal et al., 2015). The CAPS method directly determines $NO_2$ concentrations based on a $NO_2$-induced phase shift measured by a photodetector. The CAPS instrument operates at a wavelength of about 450 nm and may overestimate $NO_2$ concentrations due to absorption of other molecules at the same wavelength (Beaver et al., 2012; Beaver et al., 2013; Kebabian et al., 2005).

Due to the different characteristics of the above three methods and demonstrated biases between the FRM and the FEM by Lamsal et al. (2015), we firstly investigate the measurement discrepancies among the above three methods. There are three sites having FRM and FEM measurements simultaneously during some periods from 2013 - 2014, two sites having both FRM and CAPS data during some periods from 2015 – 2016, and one site using all three measurement methods during some periods in 2015. Figure S4 shows the hourly averaged ratios of FEM and CAPS to FRM data, respectively, for 4 seasons during 2013 – 2016. The CAPS/FRM ratios are in the range of 0.94 – 1.06 and the FEM/FRM ratios of 0.86 – 1.11. Furthermore, Zhang et al. (2018) discussed that the relative trends are not affected by scaling the observation data. As in the work by Zhang et al. (2018), we analyze the relative trends in the surface $NO_2$ data. We, therefore, did not scale the FRM data. At sites with FEM or CAPS measurements, we use these measurements in place of FRM data. If both FEM and CAPS data are available, we use the averages of the two datasets.

Since $NO_2$ surface concentrations have significant diurnal variations (Figure S5), we choose the data at 9:00-10:00 LT for comparison with GOME-2A/2B data, 10:00-11:00 LT for comparison with SCIAMACHY data, and 13:00-14:00 LT for OMI data. The seasonal $RCI <$ 50% requirement is also used here to be consistent with the analysis of satellite TVCD data, and thus about 1.5% of the data are removed. We also require that the measurement site must have

valid measurements in the aforementioned 3 hours for at least one season from 2003 – 2017. The locations of the 179 selected sites using the site selection criteria are shown in Figure 1. The region definitions follow the U.S. Census Bureau (https://www2.census.gov/geo/pdfs/maps-data/maps/reference/us_regdiv.pdf).

# 3. Results and Discussions

## 3.1 Nonlinear relationships among anthropogenic $NO_x$ emissions, $NO_2$ surface concentrations, and $NO_2$ TVCDs

$NO_2$ surface concentrations and $NO_2$ TVCD are not linearly correlated with $NO_x$ emissions due to chemical nonlinearity, $NO_2$ hydrolysis on aerosols ($NO_2 \xrightarrow{aerosol,\ H_2O} 0.5HNO_3 + 0.5HNO_2$), dry deposition, transport effects, and background sources (Gu et al., 2013; Lamsal et al., 2011). Therefore, it is necessary to first investigate the nonlinearities among $NO_x$ emissions, $NO_2$ surface concentrations, and TVCDs over the CONUS before we compare the trends between $NO_2$ surface concentrations and TVCDs. The nonlinearity between $NO_x$ emission and $NO_2$ TVCD is analyzed by examining the local sensitivity of $NO_2$ TVCD to $NO_x$ emissions (Gu et al., 2013; Lamsal et al., 2011; Tong et al., 2015), which is defined as β in Equation (1). We further define γ as the sensitivity of $NO_2$ surface concentration to $NO_x$ emission:

$$\frac{\Delta E}{E} = \beta \frac{\Delta \Omega}{\Omega} \quad (1)$$

$$\frac{\Delta E}{E} = \gamma \frac{\Delta c}{c} \quad (2)$$

where $E$ denotes $NO_x$ emission and $\Delta E$ denotes the change of $NO_x$ emission; $\Omega$ denotes $NO_2$ TVCD, $c$ denotes surface $NO_2$ concentration, and $\Delta\Omega$ and $\Delta c$ denote the corresponding changes.

We computed β and γ values for July 2011 over the CONUS using REAM. To compute local β and γ values, we added another independent group of chemistry species ("group 2") in REAM in order to compute the standard and sensitivity simulations concurrently. The original chemical species in the model ("group 1") were used in the standard simulation. For group 2 chemical species, anthropogenic $NO_x$ emissions were reduced by 15%. In the model simulation, we first computed the advection of group 1 tracers. The horizontal tracer fluxes were therefore available. All influxes into a grid cell for group 2 tracer simulation were from group 1 tracer simulation; only outfluxes were computed using group 2 tracers. The outflux was one way in that nitrogen species were transported out but the transport did not affect adjacent grid cells because the influxes were from group 1 tracer simulation. Using this procedure, the effects of anthropogenic $NO_x$ emission reduction were localized. The β and γ values were computed by the ratio of TVCD and surface concentration changes to 15% change of anthropogenic $NO_x$ emissions, respectively.

Figure 2 shows the distributions of our β and γ ratios as a function of anthropogenic $NO_x$ emissions for July 2011 over the CONUS. Results essentially the same as Figure 2 were obtained when a perturbation of 10% was used for anthropogenic $NO_x$ emissions. Figure S6 shows the distributions of $NO_2$ TVCD fraction in the boundary layer at 13:00 – 14:00 LT and 10:00 – 11:00 LT, and the fraction of soil $NO_x$ emissions in all surface sources (soil + anthropogenic) on weekdays for July 2011, respectively. In Figure S7, we analyzed the contributions of background sources, chemical nonlinearity, and other factors (transport, $NO_2$ hydrolysis on aerosols, and dry deposition) to the nonlinear relationships (β and γ) among anthropogenic $NO_x$ emissions, $NO_2$ surface concentrations, and $NO_2$ TVCDs. While the model simulation is for one summer month, several key points on the surface and column concentration sensitivities to anthropogenic $NO_x$ emissions have implications for comparing the trends of AQS and satellite TVCD data. (1) Both β and γ values are negatively correlated with anthropogenic $NO_x$ emissions due to chemical

nonlinearity, transport, and background $NO_x$ contributions (Figures 2, S6, and S7) (Gu et al., 2016; Lamsal et al., 2011). It is consistent with the distribution of β as a function of $NO_x$ emissions in China (Gu et al., 2013), although the β ratios for the US are generally larger than for China due primarily to different emission distributions of $NO_x$ and VOCs and regional circulation patterns (Zhao et al., 2009b). (2) The uncertainties of β and γ values increase significantly as anthropogenic $NO_x$ emissions decrease, which means regions with low anthropogenic $NO_x$ emissions are more sensitive to environmental conditions, such as $NO_x$ transport from nearby regions which may even produce negative β and γ values (Figures 2 and S7). (3) The value of γ is generally less than β, especially for low-anthropogenic-$NO_x$ emission regions, which reflects the significant contribution of free tropospheric $NO_2$ to $NO_2$ TVCD but not to $NO_2$ surface concentrations (Figures 2, S6, and S7). (4) Generally, the standard deviations of β and γ tend to be larger at 10:00 – 11:00 than at 13:00 – 14:00 LT, reflecting a stronger transport effect due to weaker chemical losses in the morning (Figures 2 and S7). (5) Both β and γ values are significantly less than 1 at 13:00 – 14:00 LT ($\beta = 0.75$ and $\gamma = 0.84$) when anthropogenic $NO_x$ emissions are $> 4 \times 10^{12}$ molecules $cm^{-2}$ $s^{-1}$, but they are close to 1 at 10:00 – 11:00 LT ($\beta = 0.97$ and $\gamma = 1.03$), which reflect stronger chemistry nonlinearity at noontime than in the morning (Figures 2 and S7). (6) Both background sources and non-emission factors contribute much more to β and γ values in low-anthropogenic-$NO_x$ emission regions than in high-anthropogenic-$NO_x$ emission regions (Figure S7). (7) Chemical nonlinearity contributes much less to β and γ values than background sources and transport effects in low-anthropogenic-$NO_x$ emission regions (Figure S7). (8) Generally, non-emission factors (mainly transport) contribute more to β and γ values than background sources in low-anthropogenic-$NO_x$ emission regions (Figures S7c and S7d) except for the first bin where background sources contribute more to β and γ values than non-emission factors at 10:00 – 11:00, which is partly caused by some grid cells with extremely low anthropogenic $NO_x$ emissions, increasing the mean contributions of background sources in the first bin.

The largely varying β and γ values for anthropogenic $NO_x$ emissions < $10^{11}$ molecules $cm^{-2}$ $s^{-1}$ imply that the trends derived from satellite TVCD data do not directly represent anthropogenic $NO_x$ emissions and that the variations of TVCD data may not be comparable to the corresponding surface $NO_2$ concentrations. We define a region "urban" if anthropogenic $NO_x$ emissions from NEI2011 are > $10^{11}$ molecules $cm^{-2}$ $s^{-1}$. All the other regions are defined as "rural". Figure 3 shows the distributions of anthropogenic $NO_x$ emissions and urban and rural regions defined in this study. Such defined urban regions account for 69.8% of the total anthropogenic $NO_x$ emissions over the CONUS, the trend of which is, therefore, representative of anthropogenic emission changes. A caveat is that some "urban" regions would become "rural" if anthropogenic $NO_x$ emissions decreased after 2011 as the EPA anthropogenic $NO_x$ emission trend suggested (Figure S2). In a sensitivity study, we define an urban region using a stricter criterion of anthropogenic $NO_x$ emissions > $2 \times 10^{11}$ molecules $cm^{-2}$ $s^{-1}$ and the analysis results are similar to those shown in the next section.

## 3.2 Trend comparisons between $NO_2$ AQS surface concentrations and coincident satellite $NO_2$ tropospheric VCD over urban and rural regions

By using anthropogenic $NO_x$ emissions of $10^{11}$ molecules $cm^{-2}$ $s^{-1}$ as the threshold value, 157 AQS sites are urban, and the rest 22 sites are rural. Their properties are summarized in Table 2. Figure 4 shows the relative annual variations of AQS $NO_2$ surface measurements at 13:00 – 14:00 and coincident OMI-QA4ECV $NO_2$ TVCD data from 2005 – 2017 in each season for urban and rural regions. The contrast between the two regions is apparent in all seasons. For comparison purposes, we scale the time series of TVCD and AQS surface $NO_2$ to their corresponding 2005 values, and the resulting data are therefore unitless. Over urban regions, $NO_2$ surface concentrations are highly correlated with $NO_2$ TVCDs (TVCD = 1.03 × AQS + 0.11, $R^2$ = 0.98), reflecting the comparable and stable β and γ values (Figure 2). However, over rural regions, the scaled TVCD data significantly deviate from AQS $NO_2$ data (TVCD = 1.15 × AQS + 0.09, $R^2$ =

0.87). It is noteworthy that the discrepancies between urban and rural data are smaller in winter than in spring, summer, and autumn due to a more dominant role of transport than chemistry and lower natural $NO_x$ emissions in winter.

We also examine the correlations of AQS $NO_2$ surface concentrations with coincident OMI-NASA, OMI-BEHR, SCIAMACHY, GOME-2A, and GOME-2B TVCD measurements. The results of OMI-NASA and OMI-BEHR are similar to those of OMI-QA4ECV (Figure 4). SCIAMACHY and GOME-2B TVCD observations at 9:00-11:00 LT also show large contrast between urban (SCIAMACHY: TVCD = 0.92 × AQS - 0.005, $R^2$ = 0.94; GOME-2B: TVCD = 0.54 × AQS + 0.56, $R^2$ = 0.96) and rural regions (SCIAMACHY: TVCD = 0.77 × AQS +0.83, $R^2$ = 0.63; GOME-2B: TVCD = 0.46 × AQS + 0.73, $R^2$ = 0.59). The correlation of coincident GOME-2A $NO_2$ TVCD data with AQS surface concentrations is poor for rural (TVCD = 0.65 × AQS + 0.56, $R^2$ = 0.44) and urban (TVCD = 0.31 × AQS + 0.56, $R^2$ = 0.21) regions (Figure S8), which likely reflects the degradation of the GOME-2A instrument causing significant increase of $NO_2$ SCD uncertainties (Boersma et al., 2018). Therefore, we excluded GOME-2A in the analysis hereafter.

We further investigate OMI-QA4ECV $NO_2$ TVCD relative annual variations from 2005 - 2017 over the regions with different anthropogenic $NO_x$ emissions in Figure 5. We find clear flattening of $NO_2$ TVCD variations as anthropogenic $NO_x$ emissions decrease, which is consistent with the above analysis. Similar to Figure 4, the spread of TVCD variation is much less in winter than the other seasons. The differences between Figures 5 and 4 are due to a much larger dataset used in the former than the latter. Only coincident AQS and OMI-QA4ECV data are used in Figure 4, but all OMI-KMNI data are used in Figure 5.

### 3.3 Trend analysis of AQS $NO_2$ surface concentrations, satellite TVCDs, and updated EPA NOx emissions

We first updated the CEMS measurement data used in the EPA $NO_x$ emission trend datasets with the newest datasets obtained from https://ampd.epa.gov/ampd/. As shown in Figure S2, the updated CEMS data lead to a reduction of anthropogenic $NO_x$ emissions during the Great Recession (2008 – 2009) and a recovery period in 2010 – 2011. The sharp drop during the Great Recession and the flattening trend right after the Great Recession are captured by OMI $NO_2$ and SCIAMACHY TVCD products (Figures 4, 6, and S9) and AQS $NO_2$ surface measurements (Figures 4, 6, and S5) and are also noted by Russell et al. (2012) and Tong et al. (2015) (Table 1).

In Figure 6, we show the comparisons among the relative variations of the updated EPA anthropogenic $NO_x$ emissions, AQS $NO_2$ surface measurements at 10:00-11:00 and 13:00-14:00, and coincident satellite $NO_2$ TVCDs for urban regions in 4 seasons from 2003 to 2017. Also shown are the comparisons among the updated EPA anthropogenic $NO_x$ emissions and satellite $NO_2$ TVCDs. There are many more data points for the latter comparison because the data selection is no longer limited to those coincident with the AQS surface data, and therefore, the uncertainty spread is much lower. The comparisons, in general, show consistent results that the updated EPA anthropogenic $NO_x$ emissions, AQS surface measurements, and satellite TVCD data are in agreement. The agreement of decreasing trends among the datasets is just as good for the post-2011 period as the pre-2011 period. This result differs from Miyazaki et al. (2017) and Jiang et al. (2018), who suggested no significant decreasing trend for OMI TVCD data and inversed $NO_x$ emissions after 2010. The disagreement can be explained by the results of Figure 5. Including the low anthropogenic $NO_x$ emission regions leads to underestimates of $NO_x$ decreases. Since the area of low anthropogenic $NO_x$ emission regions is larger than high anthropogenic $NO_x$ emission regions (Table 2), the arithmetic averaging will lead to a large weighting of rural observations, which do not reflect anthropogenic $NO_x$ emission changes. Miyazaki et al. (2017)

and Jiang et al. (2018) included all regions in their analyses, but we exclude rural regions. Figure S9 shows the seasonal variations if the TVCDs over rural regions are included; the result shows a much lower decreasing rate of TVCDs over the CONUS. The much slower satellite TVCD trends for regions with low $NO_x$ emissions was previously discussed by Zhang et al. (2018). In addition, Miyazaki et al. (2017) and Jiang et al. (2018) conducted $NO_x$ emission inversions by using the Model for Interdisciplinary Research on Climate (MIROC)-Chem with a coarse resolution of 2.8° × 2.8°, which was insufficient to separate urban and rural regions and might distort predicted $NO_2$ TVCDs and inversed $NO_x$ emissions due to nonlinear effects (Valin et al., 2011; Yu et al., 2016), which is another possible reason for their find of flattening $NO_x$ emission trends after 2010.

We summarize the decreasing rates of $NO_2$ after the Great Recession in Table 3. To minimize the effect of the sharp decrease and the subsequent recovery, we chose to analyze the post-2011 period. Table 3 summarizes the results for each season, while Table 1 gives the averaged annual decreasing trends. Generally, Tables 1 and 3 confirm the continuous decreases of AQS surface observations, satellite $NO_2$ TVCD, and updated EPA anthropogenic $NO_x$ emissions after 2011 as in Figure 6, but the decreasing rates are lower than the pre-2011 period. Over the AQS urban sites, the slowdown magnitudes are 9% for AQS surface observations and 20% - 40% for satellite $NO_2$ TVCD measurements, which may reflect in part smaller $\gamma$ than $\beta$ values (Table 2). Our estimated slowdown magnitudes are significantly lower than Lamsal et al. (2015) and Jiang et al. (2018) (Table 1), which might be caused by their different data processing methods, such as including AQS sites with incomplete measurement records (Silvern et al., 2019).

Over the CONUS urban regions, updated EPA anthropogenic $NO_x$ emissions show a slowdown of 22% compared to 29% - 46% for three OMI $NO_2$ TVCD products. The difference is partially due to the $\beta$ ratio of 2.5 ± 1.0 at 13:00 – 14:00 over the CONUS urban regions (Table 2). Satellite $NO_2$ TVCD measurement uncertainties also contribute to the difference. From 2013 – 2017, GOME-2B $NO_2$ TVCDs decrease more than OMI products, especially in spring, autumn

and winter (Tables 1 and 3). Finally, trend analyses in different regions (Figure 7 and Table S4) indicate that generally, the Midwest has the least slowdown of the decreasing rate for urban OMI $NO_2$ TVCD (-14% on average) after 2011 compared to the Northeast (-30%), South (-34%), and West (-28%).

The results presented in this study are qualitatively in agreement with the work by Silvern et al. (2019). The two studies were independent. Therefore, the foci of the studies are different despite reaching similar conclusions. While we focused on understanding the detailed data analysis of Jiang et al. (2018) and limited the use of model simulation results so that our results can be compared to the previous study directly, Silvern et al. (2019) relied more on multi-year model simulations. As a result, Silvern et al. (2019) can clearly identify the contributions of the $NO_2$ columns by natural emissions and make use of additional observations such as nitrate deposition fluxes. They also identified model biases in simulating the trends of $NO_2$ TVCDs by missing natural emissions in the free troposphere. Our study, on the other hand, explored the data analysis procedure through which the trend of anthropogenic emissions can be derived from satellite observations and its limitations.

# 4. Conclusions

Using model simulations for July 2017, we demonstrate the nonlinear relationship of $NO_2$ surface concentration and TVCD with anthropogenic $NO_x$ emissions. Over low anthropogenic $NO_x$ emission regions, the ratios of anthropogenic $NO_x$ emission changes to the changes of surface concentrations ($\gamma$) and TVCDs ($\beta$) have very large variations and $\beta > \gamma \gg 1$. Therefore, for the same emission changes, surface concentration and TVCD changes are much smaller and variable than urban regions, making it difficult to use the observations to directly infer anthropogenic $NO_x$ emission trends. We find that defining urban regions where anthropogenic $NO_x$ emissions are > $10^{11}$ molecules $cm^{-2}$ $s^{-1}$ and using surface and TVCD

observations over these regions can infer the trends that can be compared with the EPA emission trend estimates.

We evaluate the anthropogenic $NO_x$ emission variations from 2003 – 2017 over the CONUS by using satellite $NO_2$ TVCD products from GOME-2B, SCIAMACHY, OMI-QA4ECV, OMI-NASA, and OMI-BEHR, over the urban regions of CONUS. We find broad agreements among the decreases of AQS $NO_2$ surface observations, satellite $NO_2$ TVCD products, and the EPA anthropogenic $NO_x$ emissions with the CEMS dataset updated. After 2011, they all show a slowdown of the decreasing rates. Over the AQS urban sites, $NO_2$ surface concentrations have a slowdown of 9% and OMI products show a slowdown of 20% - 40%. Over the CONUS urban regions, OMI TVCD products indicate a slowdown of 29% - 46%, and the updated EPA anthropogenic $NO_x$ emissions have a slowdown of 22%. The different slowdown magnitudes between OMI TVCD products and the other two datasets may be caused by the nonlinear response of TVCD to anthropogenic emissions and the uncertainties of satellite measurements (e.g., GOME-2B TVCD data show a larger decreasing trend than OMI products from 2013 – 2017).

We did not find observation evidence supporting the notion that anthropogenic $NO_x$ emissions have not been decreasing after the Great Recession. In future studies, we recommend that the nonlinear relationships of $NO_x$ emissions with $NO_2$ TVCD and surface concentration be carefully evaluated when applying satellite and surface measurements to infer the changes of anthropogenic $NO_x$ emissions.

## Data availability

The EPA AQS hourly surface $NO_2$ measurements are downloaded from https://aqs.epa.gov/aqsweb/airdata/download_files.html#Raw. QA4ECV 1.1 $NO_2$ VCD products

(OMI-QA4ECV, GOME-2A, and SCIAMACHY) are from http://temis.nl/qa4ecv/no2col/data/. GOME-2B $NO_2$ VCD products are from http://www.temis.nl/airpollution/no2col/no2colgome2b.php. OMI-BEHR and OMI-NASA archives are from http://behr.cchem.berkeley.edu/DownloadBEHRData.aspx. REAM simulation results for this study are available upon request.

## Author contribution

JL and YW designed the study. JL conducted model simulations and data analyses with discussions with YW. JL and YW wrote the manuscript.

## Competing interests

The authors declare that they have no conflict of interest.

## Acknowledgments

This work was supported by the NASA ACMAP Program. We thank Ruixiong Zhang for discussions with J. Li. Thank Benjamin Wells, Alison Eyth, Lee Tooly from EPA, the EPA MOVES team, Betty Carter from COORDINATING RESEARCH COUNCIL, INC., Brain McDonald from NOAA, and Zhe Jiang from University of Science and Technology of China for helping us an understanding of the NEI MOVES mobile source emissions.

## References

Alkuwari, F. A., Guillas, S., and Wang, Y.: Statistical downscaling of an air quality model using Fitted Empirical Orthogonal Functions, Atmos. Environ., 81, 1-10, https://doi.org/10.1016/j.atmosenv.2013.08.031, 2013.

Beaver, M., Long, R., and Kronmiller, K.: Characterization and Development of Measurement Methods for Ambient Nitrogen Dioxide ($NO_2$), National Air Quality Conference - Ambient Air Monitoring 2012, Denver, CO, US, 2012.

Beaver, M., Kronmiller, K., Duvall, R., Kaushik, S., Morphy, T., King, P., and Long, R.: Direct and Indirect Methods for the Measurement of Ambient Nitrogen Dioxide, AWMA Measurement Technologies meeting, Sacramento, CA, US, 2013.

Beirle, S., Platt, U., Wenig, M., and Wagner, T.: Weekly cycle of $NO_2$ by GOME measurements: A signature of anthropogenic sources, Atmos. Chem. Phys., 3, 2225-2232, https://doi.org/10.5194/acp-3-2225-2003, 2003.

Bishop, G. A., and Stedman, D. H.: Reactive nitrogen species emission trends in three light-/medium-duty United States fleets, Environ. Sci. Technol., 49, 11234-11240, https://doi.org/10.1021/acs.est.5b02392, 2015.

Boersma, K. F., Eskes, H. J., Richter, A., De Smedt, I., Lorente, A., Beirle, S., van Geffen, J. H., Zara, M., Peters, E., and Roozendael, M. V.: Improving algorithms and uncertainty estimates for satellite $NO_2$ retrievals: results from the quality assurance for the essential climate variables (QA4ECV) project, Atmos. Meas. Tech., 11, 6651-6678, https://doi.org/10.5194/amt-11-6651-2018, 2018.

Cheng, Y., Wang, Y., Zhang, Y., Chen, G., Crawford, J. H., Kleb, M. M., Diskin, G. S., and Weinheimer, A. J.: Large biogenic contribution to boundary layer $O_3$-CO regression slope in summer, Geophys. Res. Lett., 44, 7061-7068, https://doi.org/10.1002/2017GL074405, 2017.

Cheng, Y., Wang, Y., Zhang, Y., Crawford, J. H., Diskin, G. S., Weinheimer, A. J., and Fried, A.: Estimator of surface ozone using formaldehyde and carbon monoxide concentrations over the eastern United States in summer, J. Geophys. Res.-Atmos., 123, 7642-7655, https://doi.org/10.1029/2018JD028452, 2018.

Choi, Y., Wang, Y., Zeng, T., Martin, R. V., Kurosu, T. P., and Chance, K.: Evidence of lightning $NO_x$ and convective transport of pollutants in satellite observations over North America, Geophys. Res. Lett., 32, https://doi.org/10.1029/2004GL021436, 2005.

Choi, Y., Wang, Y., Yang, Q., Cunnold, D., Zeng, T., Shim, C., Luo, M., Eldering, A., Bucsela, E., and Gleason, J.: Spring to summer northward migration of high $O_3$ over the western North Atlantic, Geophys. Res. Lett., 35, https://doi.org/10.1029/2007GL032276, 2008a.

Choi, Y., Wang, Y., Zeng, T., Cunnold, D., Yang, E. S., Martin, R., Chance, K., Thouret, V., and Edgerton, E.: Springtime transitions of $NO_2$, CO, and $O_3$ over North America: Model evaluation and analysis, J. Geophys. Res.-Atmos., 113, https://doi.org/10.1029/2007JD009632, 2008b.

Choi, Y., Kim, H., Tong, D., and Lee, P.: Summertime weekly cycles of observed and modeled $NO_x$ and $O_3$ concentrations as a function of satellite-derived ozone production sensitivity and land use types over the Continental United States, Atmos. Chem. Phys., 12, 6291-6307, https://doi.org/10.5194/acp-12-6291-2012, 2012.

Crouse, D. L., Peters, P. A., Hystad, P., Brook, J. R., van Donkelaar, A., Martin, R. V., Villeneuve, P. J., Jerrett, M., Goldberg, M. S., and Pope III, C. A.: Ambient $PM_{2.5}$, $O_3$, and $NO_2$ exposures and associations with mortality over 16 years of follow-up in the Canadian Census Health and Environment Cohort (CanCHEC), Environ. Health Perspect., 123, 1180, https://doi.org/10.1289/ehp.1409276, 2015.

De Gouw, J. A., Parrish, D. D., Frost, G. J., and Trainer, M.: Reduced emissions of CO2, $NO_x$, and $SO_2$ from US power plants owing to switch from coal to natural gas with combined cycle technology, Earth's Future, 2, 75-82, https://doi.org/10.1002/2013EF000196, 2014.

Drosoglou, T., Bais, A. F., Zyrichidou, I., Kouremeti, N., Poupkou, A., Liora, N., Giannaros, C., Koukouli, M. E., Balis, D., and Melas, D.: Comparisons of ground-based tropospheric $NO_2$ MAX-DOAS measurements to satellite observations with the aid of an air quality model over the Thessaloniki area, Greece, Atmos. Chem. Phys., 17, 5829-5849, https://doi.org/10.5194/acp-17-5829-2017, 2017.

Drosoglou, T., Koukouli, M. E., Kouremeti, N., Bais, A. F., Zyrichidou, I., Balis, D., Xu, J., and Li, A.: MAX-DOAS $NO_2$ observations over Guangzhou, China; ground-based and satellite comparisons, Atmos. Meas. Tech., 11, 2239-2255, https://doi.org/10.5194/amt-11-2239-2018, 2018.

EPA: PROFILE OF VERSION 1 OF THE 2014 NATIONAL EMISSIONS INVENTORY, U.S. Environmental Protection Agency, 2017.

Air Pollutant Emissions Trends Data: https://www.epa.gov/air-emissions-inventories/air-pollutant-emissions-trends-data, 2018.

Fisher, J. A., Jacob, D. J., Travis, K. R., Kim, P. S., Marais, E. A., Chan Miller, C., Yu, K., Zhu, L., Yantosca, R. M., and Sulprizio, M. P.: Organic nitrate chemistry and its implications for nitrogen budgets in an isoprene-and monoterpene-rich atmosphere: constraints from aircraft ($SEAC^4RS$) and ground-based (SOAS) observations in the Southeast US, Atmos. Chem. Phys., 16, 5969-5991, https://doi.org/10.5194/acp-16-5969-2016, 2016.

Georgoulias, A. K., van der A, R. J., Stammes, P., Boersma, K. F., and Eskes, H. J.: Trends and trend reversal detection in 2 decades of tropospheric $NO_2$ satellite observations, Atmos. Chem. Phys., 19, 6269-6294, https://doi.org/10.5194/acp-19-6269-2019, 2019.

Greenberg, N., Carel, R. S., Derazne, E., Bibi, H., Shpriz, M., Tzur, D., and Portnov, B. A.: Different effects of long-term exposures to $SO_2$ and $NO_2$ air pollutants on asthma severity in young adults, J. Toxicol. Environ. Health, A, 79, 342-351, https://doi.org/10.1080/15287394.2016.1153548, 2016.

Greenberg, N., Carel, R. S., Derazne, E., Tiktinsky, A., Tzur, D., and Portnov, B. A.: Modeling long-term effects attributed to nitrogen dioxide ($NO_2$) and sulfur dioxide ($SO_2$) exposure on asthma morbidity in a nationwide cohort in Israel, J. Toxicol. Environ. Health, A, 80, 326-337, https://doi.org/10.1080/15287394.2017.1313800, 2017.

Gu, D., Wang, Y., Smeltzer, C., and Liu, Z.: Reduction in $NO_x$ emission trends over China: Regional and seasonal variations, Environ. Sci. Technol., 47, 12912-12919, https://doi.org/10.1021/es401727e, 2013.

Gu, D., Wang, Y., Smeltzer, C., and Boersma, K. F.: Anthropogenic emissions of $NO_x$ over China: Reconciling the difference of inverse modeling results using GOME-2 and OMI measurements, J. Geophys. Res.-Atmos., 119, 7732-7740, https://doi.org/10.1002/2014JD021644, 2014.

514 Gu, D., Wang, Y., Yin, R., Zhang, Y., and Smeltzer, C.: Inverse modelling of $NO_x$ emissions over
515 eastern China: uncertainties due to chemical non-linearity, Atmos. Meas. Tech., 9, 5193-5201,
516 https://doi.org/10.5194/amt-9-5193-2016, 2016.

517 Guenther, A. B., Jiang, X., Heald, C. L., Sakulyanontvittaya, T., Duhl, T., Emmons, L. K., and
518 Wang, X.: The Model of Emissions of Gases and Aerosols from Nature version 2.1
519 (MEGAN2.1): an extended and updated framework for modeling biogenic emissions, Geosci.
520 Model Dev., 5, 1471-1492, https://doi.org/10.5194/gmd-5-1471-2012, 2012.

521 Hassler, B., McDonald, B. C., Frost, G. J., Borbon, A., Carslaw, D. C., Civerolo, K., Granier, C.,
522 Monks, P. S., Monks, S., and Parrish, D. D.: Analysis of long-term observations of $NO_x$ and CO
523 in megacities and application to constraining emissions inventories, Geophys. Res. Lett., 43,
524 9920-9930, https://doi.org/10.1002/2016GL069894, 2016.

525 Heinrich, J., Thiering, E., Rzehak, P., Krämer, U., Hochadel, M., Rauchfuss, K. M., Gehring, U.,
526 and Wichmann, H.-E.: Long-term exposure to $NO_2$ and $PM_{10}$ and all-cause and cause-specific
527 mortality in a prospective cohort of women, Occup. Environ. Med., 70, 179-186,
528 https://doi.org/10.1136/oemed-2012-100876, 2013.

529 Jiang, Z., McDonald, B. C., Worden, H., Worden, J. R., Miyazaki, K., Qu, Z., Henze, D. K.,
530 Jones, D. B. A., Arellano, A. F., and Fischer, E. V.: Unexpected slowdown of US pollutant
531 emission reduction in the past decade, Proc. Natl. Acad. Sci. U.S.A., 201801191,
532 https://doi.org/10.1073/pnas.1801191115, 2018.

533 Kampa, M., and Castanas, E.: Human health effects of air pollution, Environ. Pollut., 151, 362-
534 367, https://doi.org/10.1016/j.envpol.2007.06.012, 2008.

535 Kebabian, P. L., Herndon, S. C., and Freedman, A.: Detection of nitrogen dioxide by cavity
536 attenuated phase shift spectroscopy, Anal. Chem., 77, 724-728,
537 https://doi.org/10.1021/ac048715y, 2005.

538 Koo, J.-H., Wang, Y., Kurosu, T. P., Chance, K., Rozanov, A., Richter, A., Oltmans, S. J.,
539 Thompson, A. M., Hair, J. W., and Fenn, M. A.: Characteristics of tropospheric ozone depletion
540 events in the Arctic spring: analysis of the ARCTAS, ARCPAC, and ARCIONS measurements
541 and satellite BrO observations, Atmos. Chem. Phys., 12, 9909-9922, https://doi.org/10.5194/acp-
542 12-9909-2012, 2012.

543 Krotkov, N. A., Lamsal, L. N., Celarier, E. A., Swartz, W. H., Marchenko, S. V., Bucsela, E. J.,
544 Chan, K. L., Wenig, M., and Zara, M.: The version 3 OMI $NO_2$ standard product, Atmos. Meas.
545 Tech., 10, 3133-3149, https://doi.org/10.5194/amt-10-3133-2017, 2017.

546 Lamsal, L. N., Martin, R. V., Padmanabhan, A., Van Donkelaar, A., Zhang, Q., Sioris, C. E.,
547 Chance, K., Kurosu, T. P., and Newchurch, M. J.: Application of satellite observations for timely
548 updates to global anthropogenic $NO_x$ emission inventories, Geophys. Res. Lett., 38,
549 https://doi.org/10.1029/2010GL046476, 2011.

550 Lamsal, L. N., Duncan, B. N., Yoshida, Y., Krotkov, N. A., Pickering, K. E., Streets, D. G., and
551 Lu, Z.: US $NO_2$ trends (2005–2013): EPA Air Quality System (AQS) data versus improved
552 observations from the Ozone Monitoring Instrument (OMI), Atmos. Environ., 110, 130-143,
553 https://doi.org/10.1016/j.atmosenv.2015.03.055, 2015.

Laughner, J. L., Zhu, Q., and Cohen, R. C.: The Berkeley High Resolution Tropospheric $NO_2$ product, Earth System Science Data, 10, 2069-2095, https://doi.org/10.5194/essd-10-2069-2018, 2018.

Li, J., Mao, J., Fiore, A. M., Cohen, R. C., Crounse, J. D., Teng, A. P., Wennberg, P. O., Lee, B. H., Lopez-Hilfiker, F. D., and Thornton, J. A.: Decadal changes in summertime reactive oxidized nitrogen and surface ozone over the Southeast United States, Atmos. Chem. Phys., 18, 2341-2361, https://doi.org/10.5194/acp-18-2341-2018, 2018.

Li, J., Wang, Y., and Qu, H.: Dependence of summertime surface ozone on $NO_x$ and VOC emissions over the United States: Peak time and value, Geophys. Res. Lett., 46, 3540-3550, https://doi.org/10.1029/2018GL081823, 2019.

Liu, Z., Wang, Y., Vrekoussis, M., Richter, A., Wittrock, F., Burrows, J. P., Shao, M., Chang, C. C., Liu, S. C., and Wang, H.: Exploring the missing source of glyoxal (CHOCHO) over China, Geophys. Res. Lett., 39, https://doi.org/10.1029/2012GL051645, 2012.

Liu, Z., Wang, Y., Costabile, F., Amoroso, A., Zhao, C., Huey, L. G., Stickel, R., Liao, J., and Zhu, T.: Evidence of aerosols as a media for rapid daytime HONO production over China, Environ. Sci. Technol., 48, 14386-14391, https://doi.org/10.1021/es504163z, 2014.

Luo, C., Wang, Y., and Koshak, W. J.: Development of a self-consistent lightning $NO_x$ simulation in large-scale 3-D models, J. Geophys. Res.-Atmos., 122, 3141-3154, https://doi.org/10.1002/2016JD026225, 2017.

McDonald, B., McKeen, S., Cui, Y. Y., Ahmadov, R., Kim, S.-W., Frost, G. J., Pollack, I., Peischl, J., Ryerson, T. B., and Holloway, J.: Modeling Ozone in the Eastern US using a Fuel-Based Mobile Source Emissions Inventory, Environ. Sci. Technol., https://doi.org/10.1021/acs.est.8b00778, 2018.

Miyazaki, K., Eskes, H., Sudo, K., Boersma, K. F., Bowman, K., and Kanaya, Y.: Decadal changes in global surface $NO_x$ emissions from multi-constituent satellite data assimilation, Atmos. Chem. Phys, 17, 807-837, https://doi.org/10.5194/acp-17-807-2017, 2017.

Myhre, G., Shindell, D., Bréon, F.-M., Collins, W., Fuglestvedt, J., Huang, J., Koch, D., Lamarque, J.-F., Lee, D., Mendoza, B., Nakajima, T., Robock, A., Stephens, G., Takemura, T., and Zhang, H.: Anthropogenic and natural radiative forcing, in: Climate change 2013: The Physical Science Basis. Contribution of Working Group I to the Fifth Assessment Report of the Intergovernmental Panel on Climate Change, Cambridge University Press, Cambridge, United Kingdom and New York, NY, USA, 659-740, 2013.

Pandey, J. S., Kumar, R., and Devotta, S.: Health risks of $NO_2$, SPM and $SO_2$ in Delhi (India), Atmos. Environ., 39, 6868-6874, https://doi.org/10.1016/j.atmosenv.2005.08.004, 2005.

Price, C., and Rind, D.: A simple lightning parameterization for calculating global lightning distributions, J. Geophys. Res.-Atmos., 97, 9919-9933, https://doi.org/10.1029/92JD00719, 1992.

Russell, A. R., Valin, L. C., and Cohen, R. C.: Trends in OMI $NO_2$ observations over the United States: effects of emission control technology and the economic recession, Atmos. Chem. Phys., 12, 12197-12209, https://doi.org/10.5194/acp-12-12197-2012, 2012.

Seinfeld, J. H., and Pandis, S. N.: Atmospheric chemistry and physics: from air pollution to climate change, John Wiley & Sons, Inc, Hoboken, New Jersey, 2016.

Silvern, R. F., Jacob, D. J., Mickley, L. J., Sulprizio, M. P., Travis, K. R., Marais, E. A., Cohen, R. C., Laughner, J. L., Choi, S., Joiner, J., and Lamsal, L. N.: Using satellite observations of tropospheric $NO_2$ columns to infer long-term trends in US $NO_x$ emissions: the importance of accounting for the free tropospheric $NO_2$ background, Atmos. Chem. Phys., 19, 8863-8878, https://doi.org/10.5194/acp-19-8863-2019, 2019.

Singh, A., and Agrawal, M.: Acid rain and its ecological consequences, J. Environ. Biol., 29, 15, 2007.

Tong, D., Lamsal, L., Pan, L., Ding, C., Kim, H., Lee, P., Chai, T., Pickering, K. E., and Stajner, I.: Long-term $NO_x$ trends over large cities in the United States during the great recession: Comparison of satellite retrievals, ground observations, and emission inventories, Atmos. Environ., 107, 70-84, https://doi.org/10.1016/j.atmosenv.2015.01.035, 2015.

Valin, L. C., Russell, A. R., Hudman, R. C., and Cohen, R. C.: Effects of model resolution on the interpretation of satellite $NO_2$ observations, Atmos. Chem. Phys., 11, 11647-11655, https://doi.org/10.5194/acp-11-11647-2011, 2011.

Wang, Y., Choi, Y., Zeng, T., Davis, D., Buhr, M., Huey, L. G., and Neff, W.: Assessing the photochemical impact of snow $NO_x$ emissions over Antarctica during ANTCI 2003, Atmos. Environ., 41, 3944-3958, https://doi.org/10.1016/j.atmosenv.2007.01.056, 2007.

Wang, Y., Beirle, S., Lampel, J., Koukouli, M., De Smedt, I., Theys, N., Ang, L., Wu, D., Xie, P., and Liu, C.: Validation of OMI, GOME-2A and GOME-2B tropospheric $NO_2$, $SO_2$ and HCHO products using MAX-DOAS observations from 2011 to 2014 in Wuxi, China: investigation of the effects of priori profiles and aerosols on the satellite products, Atmos. Chem. Phys., 17, 5007, https://doi.org/10.5194/acp-17-5007-2017, 2017.

Weinmayr, G., Romeo, E., De Sario, M., Weiland, S. K., and Forastiere, F.: Short-term effects of $PM_{10}$ and $NO_2$ on respiratory health among children with asthma or asthma-like symptoms: a systematic review and meta-analysis, Environ. Health Perspect., 118, 449-457, https://doi.org/10.1289/ehp.0900844, 2009.

Xing, J., Pleim, J., Mathur, R., Pouliot, G., Hogrefe, C., Gan, C. M., and Wei, C.: Historical gaseous and primary aerosol emissions in the United States from 1990 to 2010, Atmos. Chem. Phys., 13, 7531-7549, https://doi.org/10.5194/acp-13-7531-2013, 2013.

Yang, Q., Wang, Y., Zhao, C., Liu, Z., Gustafson Jr, W. I., and Shao, M.: $NO_x$ emission reduction and its effects on ozone during the 2008 Olympic Games, Environ. Sci. Technol., 45, 6404-6410, https://doi.org/10.1021/es200675v, 2011.

Yienger, J. J., and Levy, H.: Empirical model of global soil-biogenic $NO_x$ emissions, J. Geophys. Res.-Atmos., 100, 11447-11464, https://doi.org/10.1029/95JD00370, 1995.

Yu, K., Jacob, D. J., Fisher, J. A., Kim, P. S., Marais, E. A., Miller, C. C., Travis, K. R., Zhu, L., Yantosca, R. M., and Sulprizio, M. P.: Sensitivity to grid resolution in the ability of a chemical

transport model to simulate observed oxidant chemistry under high-isoprene conditions, Atmos. Chem. Phys., 16, 4369-4378, https://doi.org/10.5194/acp-16-4369-2016, 2016.

Zara, M., Boersma, K. F., De Smedt, I., Richter, A., Peters, E., Van Geffen, J. H. G. M., Beirle, S., Wagner, T., Van Roozendael, M., and Marchenko, S.: Improved slant column density retrieval of nitrogen dioxide and formaldehyde for OMI and GOME-2A from QA4ECV: intercomparison, uncertainty characterization, and trends, Meas. Tech. Discuss, 1-47, https://doi.org/10.5194/amt-11-4033-2018, 2018.

Zhang, R., Wang, Y., He, Q., Chen, L., Zhang, Y., Qu, H., Smeltzer, C., Li, J., Alvarado, L., and Vrekoussis, M.: Enhanced trans-Himalaya pollution transport to the Tibetan Plateau by cut-off low systems, Atmos. Chem. Phys., 17, 3083-3095, https://doi.org/10.5194/acp-17-3083-2017, 2017.

Zhang, R., Wang, Y., Smeltzer, C., Qu, H., Koshak, W., and Boersma, K. F.: Comparing OMI-based and EPA AQS in situ $NO_2$ trends: towards understanding surface $NO_x$ emission changes, Atmos. Meas. Tech., 11, 3955-3967, https://doi.org/10.5194/amt-11-3955-2018, 2018.

Zhang, Y., and Wang, Y.: Climate-driven ground-level ozone extreme in the fall over the Southeast United States, Proc. Natl. Acad. Sci. U.S.A., 113, 10025-10030, https://doi.org/10.1073/pnas.1602563113, 2016.

Zhao, C., and Wang, Y.: Assimilated inversion of $NO_x$ emissions over east Asia using OMI $NO_2$ column measurements, Geophys. Res. Lett., 36, https://doi.org/10.1029/2008GL037123, 2009.

Zhao, C., Wang, Y., Choi, Y., and Zeng, T.: Summertime impact of convective transport and lightning $NO_x$ production over North America: modeling dependence on meteorological simulations, Atmos. Chem. Phys., 9, 4315-4327, https://doi.org/10.5194/acp-9-4315-2009, 2009a.

Zhao, C., Wang, Y., and Zeng, T.: East China plains: A "basin" of ozone pollution, Environ. Sci. Technol., 43, 1911-1915, https://doi.org/10.1021/es8027764, 2009b.

Zhao, C., Wang, Y., Yang, Q., Fu, R., Cunnold, D., and Choi, Y.: Impact of East Asian summer monsoon on the air quality over China: View from space, J. Geophys. Res.-Atmos., 115, https://doi.org/10.1029/2009JD012745, 2010.

**Table 1.** Summary of trends of satellite $NO_2$ TVCD products, $NO_2$ surface measurements, and EPA anthropogenic $NO_x$ emissions during from different studies

| Studies | Datasets | Period 1[1] | | Period 2 | | Period 3 | | Slowdown ratio[3] |
|---|---|---|---|---|---|---|---|---|
| | | Time | Trend ($yr^{-1}$)[2] | Time | Trend ($yr^{-1}$) | Time | Trend ($yr^{-1}$) | |
| This study for CONUS "urban" sites[4] | GOME-2B[5] (36 × 36 $km^2$) | | | | | 2013 - 2017 | **-8.2 ± 3.0%** | |
| | SCIAMACHY (36 × 36 $km^2$) | 2003 – 2011 | **-6.3 ± 1.1%** | | | | | |
| | OMI-NASA (36 × 36 $km^2$) | 2005 – 2011 | **-8.6 ± 1.2%** | | | 2011 – 2016 | **-6.1 ± 3.6%** | **-29%**[2] |
| | OMI-BEHR (36 × 36 $km^2$) | 2005 – 2011 | **-8.2 ± 1.3%** | | | 2011 – 2016 | **-4.4 ± 1.6%** | **-46%** |
| | OMI-QA4ECV (36 × 36 $km^2$) | 2005 – 2011 | **-7.7 ± 1.4%** | | | 2011 - 2017 | **-4.2 ± 0.5%** | **-46%** |
| | Updated EPA $NO_x$ emissions[6] | 2003 – 2011 | **-6.5 ± 0.8%** | | | 2011 - 2017 | **-5.1 ± 0.3%** | **-22%** |
| This study for AQS "urban" sites | GOME-2B (36 × 36 $km^2$) | | | | | 2013 - 2017 | **-10.2 ± 2.9%** | |
| | SCIAMACHY (36 × 36 $km^2$) | 2003 - 2011 | **-7.6 ± 1.1%** | | | | | |
| | OMI-NASA (36 × 36 $km^2$) | 2005 - 2011 | **-9.0 ± 0.8%** | | | 2011 – 2016 | **-7.2 ± 3.8%** | **-20%** |
| | OMI-BEHR (36 × 36 $km^2$) | 2005 - 2011 | **-8.9 ± 0.3%** | | | 2011 – 2016 | **-6.2 ± 2.6%** | **-30%** |
| | OMI-QA4ECV (36 × 36 $km^2$) | 2005 - 2011 | **-9.0 ± 0.8%** | | | 2011 - 2017 | **-5.4 ± 0.9%** | **-40%** |
| | $NO_2$ surface VMR[7] | 2003 - 2011 | **-6.5 ± 1.2%** | | | 2011 - 2017 | **-5.9 ± 0.8%** | **-9%** |
| (Russell et al., 2012)[8] | BEHR v2.1 $NO_2$ TVCD (0.05°×0.05°) | 2005 - 2007 | -6 ± 5% **(-6.2%)**[9] | 2007 - 2009 | -8 ± 5% **(-8.4%)** | 2009 - 2011 | -3 ± 4% **(-3.0%)** | **-52%** |
| | Updated EPA $NO_x$ emissions | | **-6.0%** | | **-10.0%** | | **-2.4%** | **-60%** |
| (Tong et al., 2015)[10] | NASA v2.1 $NO_2$ TVCD (pixels < 50 × 24 $km^2$) | 2005 - 2007 | -7.3% **(-7.6%)** | 2008 - 2009 | -9.2% **(-11.4%)** | 2010 - 2012 | -2.8% **(-4.4%)** | **-42%** |
| | BEHR v2.1 $NO_2$ TVCD (pixels < 50 × 24 $km^2$) | | -8.9% **(-9.3%)** | | -9.1% **(-11.8%)** | | -3.6% **(-6.0%)** | **-35%** |
| | $NO_2$ surface VMR | | -6.0% **(-6.2%)** | | -10.8% **(-13.2%)** | | -3.4% **(-5.4%)** | **-13%** |
| | Updated EPA $NO_x$ emissions | | **-6.0%** | | **-10.0%** | | **-3.4%** | **-43%** |
| (Lamsal et al., 2015)[11] | NASA v2.1 $NO_2$ TVCD (0.1°×0.1°) | 2005 - 2008 | -4.8 ± 1.9% **(-5.1%)** | | | 2010 - 2013 | -1.2 ± 1.2% **(-1.2%)** | **-76%** |
| | $NO_2$ surface VMR | | -3.7 ± 1.5% **(-3.8%)** | | | | -2.1 ± 1.4% **(-2.1%)** | **-45%** |
| | Updated EPA $NO_x$ emissions | | **-6.4%** | | | | **-4.0%** | **-38%** |
| (Jiang et al., 2018)[11] | NASA v3 $NO_2$ TVCD (0.5°×0.667°) | 2005 - 2009 | -10.2 ± 1.8% **(-9.8%)** | | | 2011-2015 | -3.2 ± 1.6% **(-3.2%)** | **-67%** |
| | QA4ECV v2 $NO_2$ TVCD (0.5°×0.667°) | | -9.6 ± 1.7% **(-9.3%)** | | | | -2.6 ± 1.8% **(-2.6%)** | **-72%** |
| | BEHR v2.1 $NO_2$ TVCD (0.5°×0.667°) | | -8.5 ± 1.8% **(-8.2%)** | | | | -2.1 ± 1.6% **(-2.1%)** | **-74%** |
| | $NO_2$ surface VMR | | -6.6 ± 1.4% **(-6.4%)** | | | | -2.6 ± 1.5% **(-2.6%)** | **-59%** |
| | Updated EPA $NO_x$ emissions | | **-7.8%** | | | | **-5.0%** | **-36%** |

[1] Since different studies used different time division methods, we list the period of each study in the table.
[2] Trends are based on an exponential model ($E(y) = E_0 \times r^{y-y_0}$: "$y$" denotes year and "$y_0$" denotes the initial year; "$E(y)$" denotes the value at year "$y$" and "$E_0$" denotes the value at the initial year; $r$-1 is the relative trend).
[3] Slowdown ratios = Trend in "period 3" / Trend in "period 1" – 1.
[4] Trends in our study are calculated based on the national seasonal trends shown in Table 3.
[5] The information on satellite products used in this study is summarized in Table S2.
[6] We updated EPA anthropogenic $NO_x$ emissions with the newest Continuous Emission Monitoring Systems (CEMS) datasets. Figure S2 shows the comparison between our updated and original EPA anthropogenic $NO_x$ emissions (EPA, 2018).
[7] Denote the averaged trends of 13:00 and 10:00 LT based on the values in Table 3.

[8] The study used $NO_2$ TVCD from urban and power plant grid cells across the U.S.

[9] Since previous studies used linear models to calculate trends and the results are sensitive to their calculation methods and the selection of initial years, we recalculate the trends based on the above exponential model, which makes all the results consistent. Our results are those bold numbers inside the parentheses, while the numbers in normal fonts are from the original publications.

[10] The study uses $NO_2$ TVCD and surface concentrations from Los Angeles, Dallas, Houston, Atlanta, Philadelphia, Washington, D.C., New York, and Boston.

[11] The two studies used the EPA Air Quality System (AQS) $NO_2$ surface measurements and coincident satellite $NO_2$ TVCD data over the U.S.

672 **Table 2.** Properties of urban and rural regions in July 2011

| type | Surface area fraction[1] | Anthropogenic $NO_x$ emissions ($\times 10^{10}$ molecules $cm^{-2}$ $s^{-1}$) | β at 13:00 – 14:00 LT | γ at 13:00 – 14:00 LT | β at 10:00 – 11:00 LT | γ at 10:00 – 11:00 LT |
|---|---|---|---|---|---|---|
| Urban/CONUS[2] | 17.3% | 29.9 | 2.5 ± 1.0 | 1.5 ± 0.4 | 2.6 ± 1.9 | 1.6 ± 1.2 |
| Rural/CONUS | 82.7% | 2.7 | 16.9 ± 16.4 | 8.5 ± 11.7 | 12.2 ± 14.0 | 6.4 ± 11.6 |
| Urban/AQS | 87.7% | 71.0 | 1.6 ± 0.8 | 1.2 ± 0.4 | 1.7 ± 1.1 | 1.3 ± 0.6 |
| Rural/AQS | 12.3% | 5.7 | 8.7 ± 9.9 | 5.2 ± 8.8 | 5.4 ± 15.1 | 3.8 ± 11.7 |

673 [1] "Fraction" denotes the percentages of "urban" or "rural" data points for the whole CONUS or all AQS sites.
674 [2] "Urban-CONUS" denote CONUS "urban" grid cells; "Urban-AQS" denote AQS "urban" site grid cells.
675
676

**Table 3.** Summary of national trends of updated EPA anthropogenic $NO_x$ emissions, AQS $NO_2$ surface concentrations at 13:00 – 14:00 and 10:00 – 11:00 LT, and satellite $NO_2$ TVCD products for 4 seasons during different periods[1]

| | | Spring | | Summer | | Autumn | | Winter | |
|---|---|---|---|---|---|---|---|---|---|
| | | AQS site | CONUS | AQS site | CONUS | AQS site | CONUS | AQS site | CONUS |
| AQS $NO_2$ VMR at 13:00 -14:00 | 2003 – 2011 | -7.3 ± 1.4% | | -7.4 ± 0.9% | | -6.7 ± 1.8% | | -5.2 ± 0.8% | |
| | 2011 – 2017 | -5.3 ± 1.6% | | -6.4 ± 1.2% | | -7.3 ± 2.5% | | -6.0 ± 2.8% | |
| AQS $NO_2$ VMR at 10:00 – 11:00 | 2003 – 2011 | -7.1 ± 1.6% | | -7.6 ± 1.5% | | -6.2 ± 2.2% | | -4.4 ± 1.6% | |
| | 2011 – 2017 | -4.4 ± 1.4% | | -6.1 ± 1.8% | | -6.3 ± 2.5% | | -5.2 ± 2.4% | |
| SCIAMACHY | 2003 – 2011 | -8.8 ± 3.4% | -6.9 ± 1.1% | -8.2 ± 1.6% | -5.2 ± 1.2% | -6.8 ± 2.4% | -5.6 ± 2.1% | -6.4 ± 7.4% | -7.5 ± 5.5% |
| | 2011 – 2017 | | | | | | | | |
| GOME2B | 2003 – 2011 | | | | | | | | |
| | 2013 – 2017 | -10.2 ± 7.8% | -8.3 ± 16.9% | -6.4 ± 14.0% | -5.3 ± 4.0% | -10.5 ± 41.6% | -6.9 ± 13.2% | -13.6 ± 15.1% | -12.3 ± 78.9% |
| OMI-QA4ECV | 2005 – 2011 | -9.3 ± 5.6% | -8.3 ± 4.6% | -8.3 ± 2.4% | -5.9 ± 5.2% | -10.0 ± 4.2% | -7.4 ± 2.4% | -8.3 ± 2.1% | -9.3 ± 5.2% |
| | 2011 – 2017 | -5.3 ± 6.0% | -4.3 ± 6.5% | -4.2 ± 3.0% | -4.9 ± 9.2% | -6.0 ± 1.8% | -3.8 ± 1.8% | -6.1 ± 25.6% | -3.8 ± 3.5% |
| OMI-NASA | 2005 – 2011 | -9.4 ± 5.0% | -9.6 ± 5.3% | -9.4 ± 2.8% | -7.1 ± 2.9% | -9.4 ± 3.2% | -8.1 ± 2.8% | -7.8 ± 3.6% | -9.5 ± 16.6% |
| | 2011 – 2016 | -4.4 ± 18.9% | -3.8 ± 7.5% | -5.7 ± 6.7% | -4.5 ± 5.3% | -6.0 ± 3.1% | -4.6 ± 3.9% | -12.8 ± 7.8% | -11.4 ± 6.6% |
| OMI-BEHR | 2005 – 2011 | -9.1 ± 5.3% | -8.9 ± 5.8% | -8.7 ± 2.4% | -6.4 ± 3.2% | -9.2 ± 3.2% | -8.0 ± 3.1% | -8.5 ± 10.6% | -9.4 ± 23.0% |
| | 2011 – 2016 | -3.8 ± 4.4% | -3.0 ± 4.0% | -5.4 ± 7.0% | -3.9 ± 6.6% | -5.6 ± 13.2% | -4.1 ± 14.0% | -9.9 ± 5.2% | -6.7 ± 5.9% |
| EPA | 2003 – 2011 | | | | -6.5 ± 0.8% | | | | |
| | 2011 – 2017 | | | | -5.1 ± 0.3% | | | | |

[1] We calculate trends by using the exponential model described in Table 1.

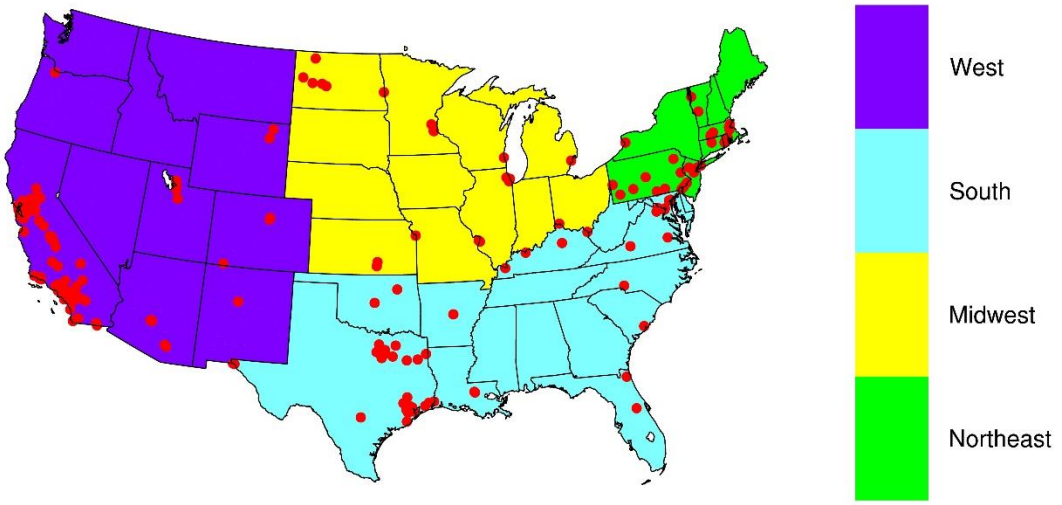


Figure 1. Region definitions and locations of $NO_2$ surface observation sites used in this study.

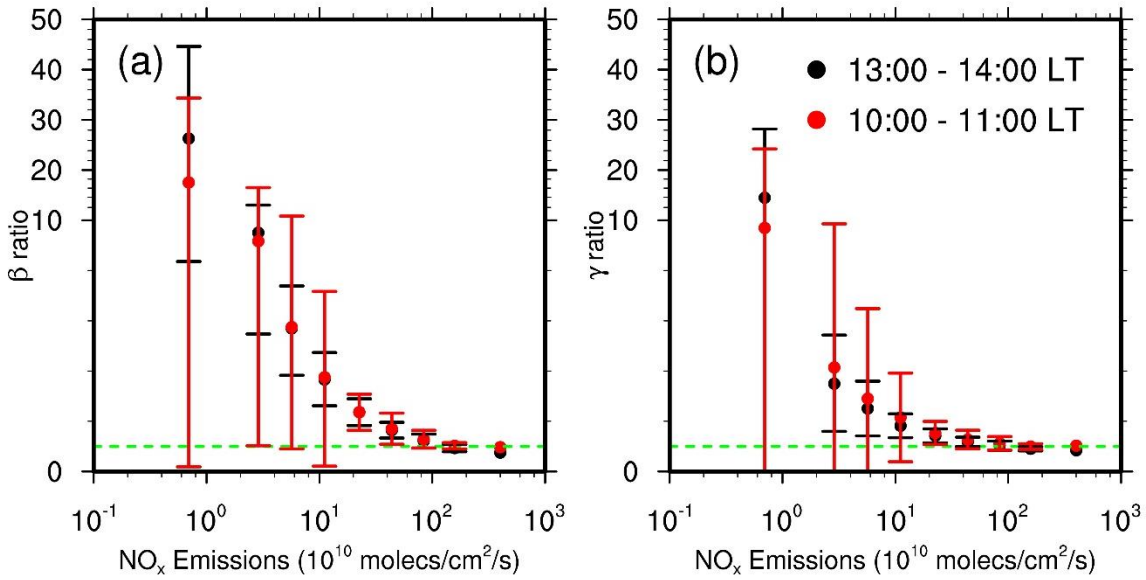


Figure 2. Distributions of β (panel a) and γ (panel b) ratios as a function of anthropogenic $NO_x$ emissions on weekdays for July 2011 over the CONUS. "13:00 – 14:00 LT" is for OMI, and "10:00 – 11:00" LT is for SCIAMACHY and GOME-2A/2B. The data are binned into nine groups based on anthropogenic $NO_x$ emissions: $E \in (0, 2^1)$, $[2^1, 2^2)$, $[2^2, 2^3)$, $[2^3, 2^4)$, $[2^4, 2^5)$, $[2^5, 2^6)$, $[2^6, 2^7)$, $[2^7, 2^8)$, $[2^8, 2^9) \times 10^{10}$ molecules $cm^{-2}$ $s^{-1}$. Here, $(0, 2^1)$ denotes $0 <$ emissions $< 2^1$, and $[2^1, 2^2)$ denotes $2^1 \leq$ emissions $< 2^2$, similar to other intervals. The green dashed line denotes a value of 1. Error bars denote standard deviations.

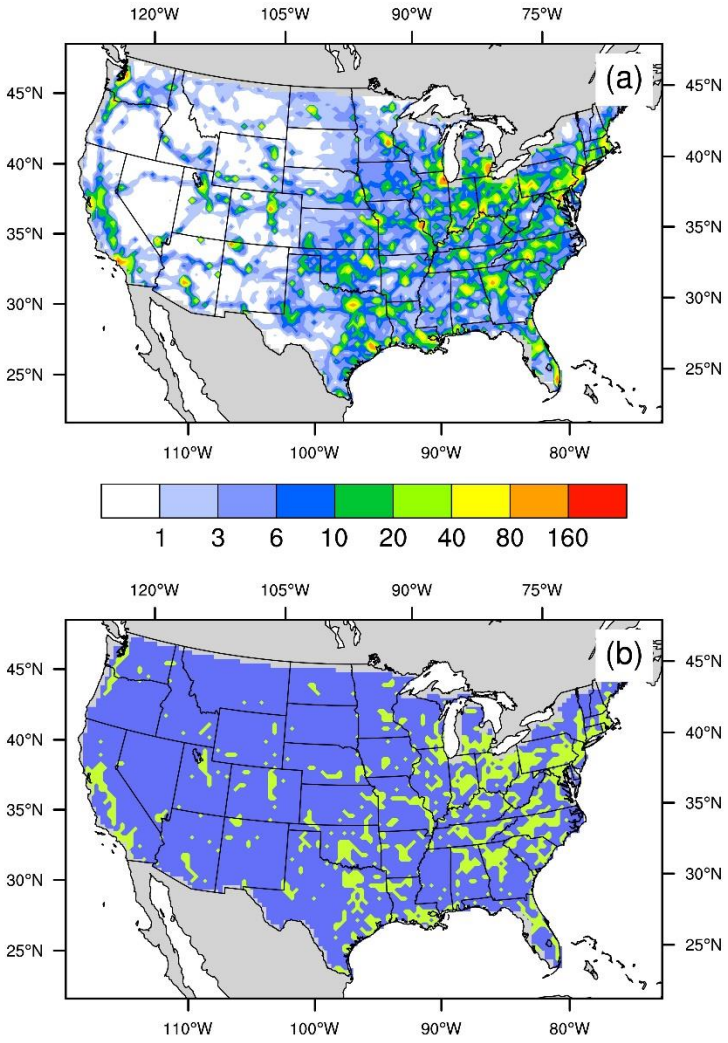


Figure 3. Spatial distributions of (a) anthropogenic $NO_x$ emissions (unit: $10^{10}$ molecules $cm^{-2}$ $s^{-1}$) and (b) "urban" regions satisfying our selection criteria. In (b), light green and blue denote the resulting urban and rural regions, respectively.

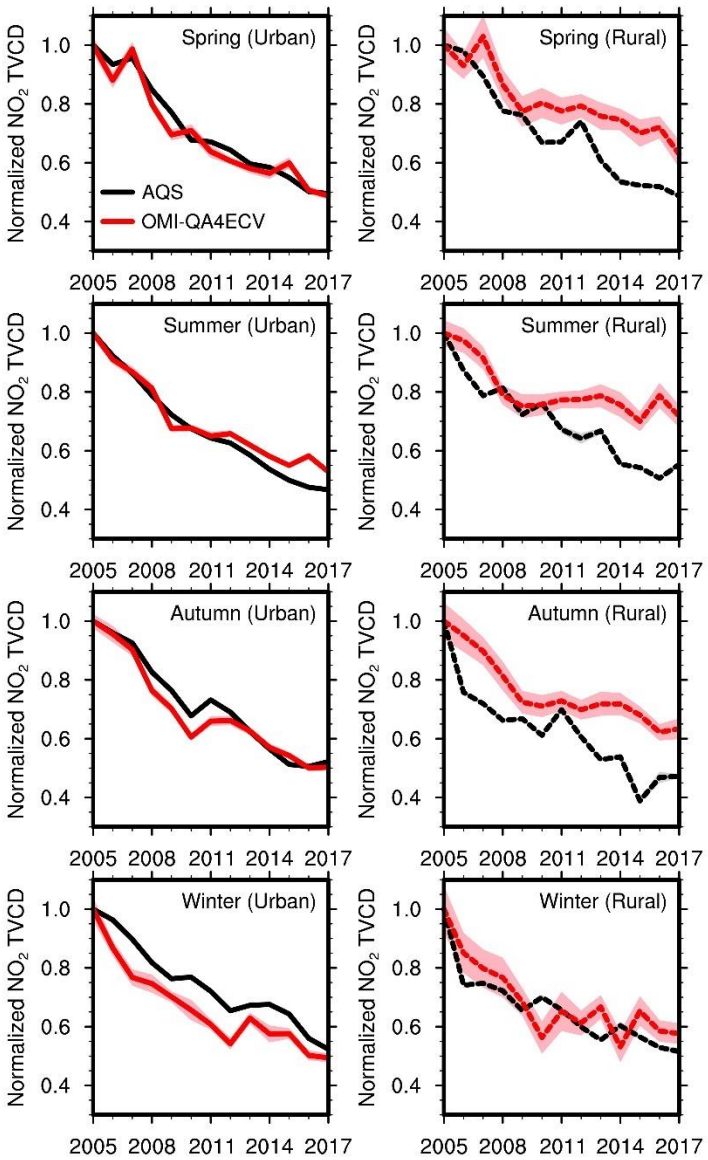


Figure 4. Relative annual variations of AQS $NO_2$ surface concentrations and coincident OMI-QA4ECV $NO_2$ TVCD in each season from 2005 – 2017 for urban (left panel) and rural (right panel) regions. The observation data are scaled by the corresponding 2005 values. Black and red lines denote AQS surface observations and OMI-QA4ECV $NO_2$ TVCDs, respectively. Shading in a lighter color is added to show the standard deviation of the results; when uncertainty is small due in part to a large number of data points, shading area may not show up.

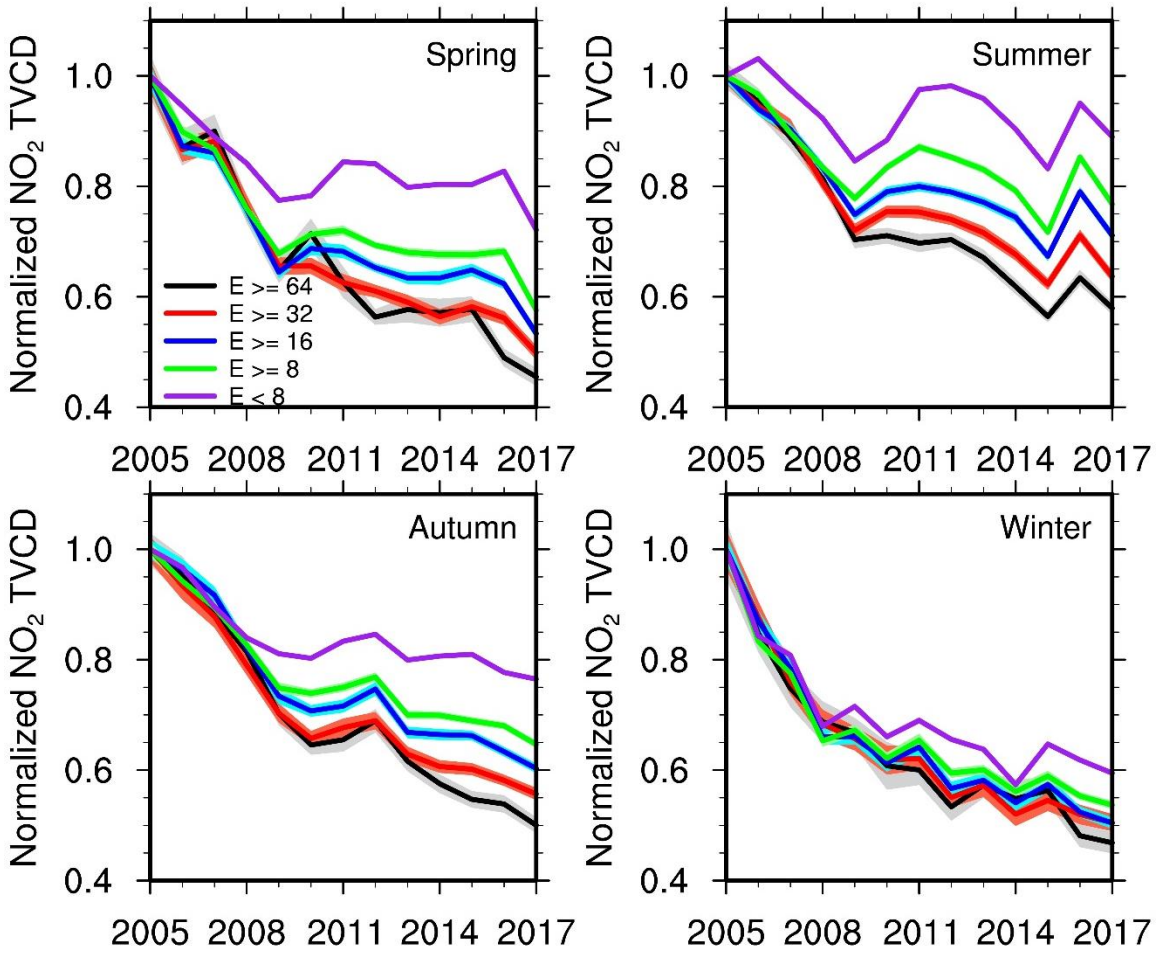


Figure 5. Relative annual variations of OMI-QA4ECV $NO_2$ TVCD for different anthropogenic $NO_x$-emission groups based on NEI2011 in each season from 2005 – 2017. "E >= 64" denotes grid cells with anthropogenic $NO_x$ emissions over $64 \times 10^{10}$ molecules $cm^{-2}$ $s^{-1}$. "E >= 32" denotes grid cells with anthropogenic $NO_x$ emissions equal to or larger than $32 \times 10^{10}$ molecules $cm^{-2}$ $s^{-1}$ but less than $64 \times 10^{10}$ molecules $cm^{-2}$ $s^{-1}$. "E >= 16" and "E >= 8" have similar meanings as "E >= 32". "E < 8" denotes grid cells with anthropogenic $NO_x$ emissions less than $8 \times 10^{10}$ molecules $cm^{-2}$ $s^{-1}$. Shading in a lighter color is added to show the standard deviation of the results; when uncertainty is small due in part to a large number of data points, shading area may not show up.

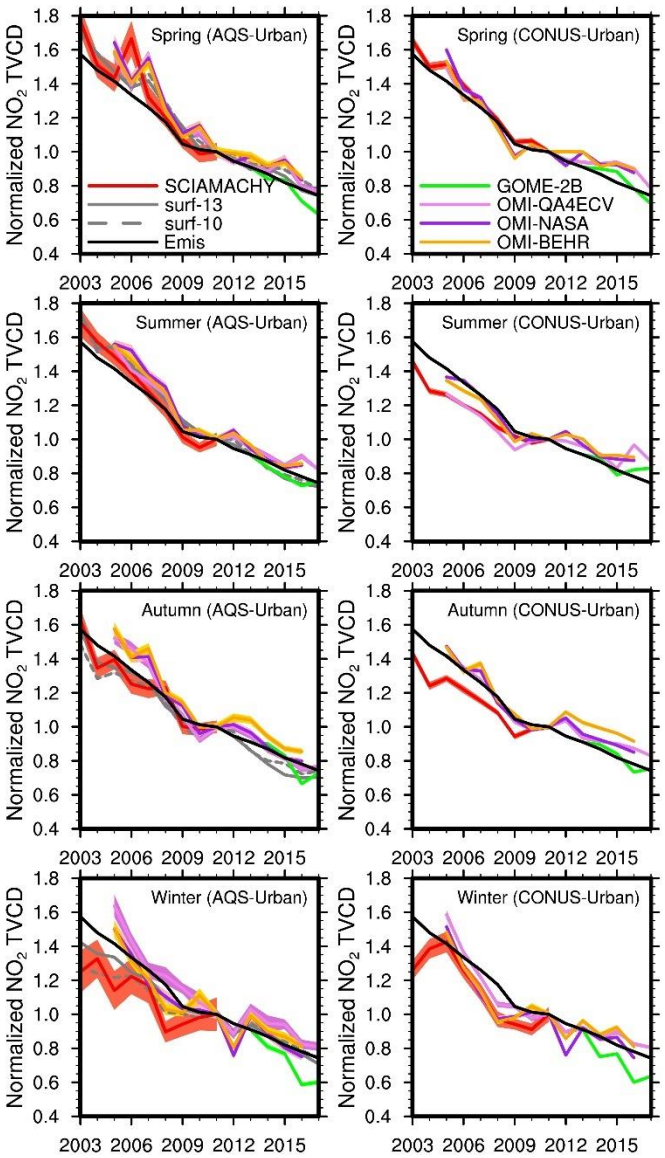


Figure 6. Relative variations of AQS $NO_2$ surface measurements at 13:00-14:00 and 10:00-11:00 LT, updated EPA anthropogenic $NO_x$ emissions, and satellite $NO_2$ TVCD data over the AQS urban sites (left column) and the CONUS urban regions (right column) for 4 seasons. AQS $NO_2$ surface measurements are not included in the right column. All datasets are scaled by their corresponding values in 2011 except for GOME-2B. For GOME-2B, we firstly normalized the values in each season to the corresponding 2013 values and plotted the relative changes from the 2013 EPA point of each season to make the GOME-2B relative variations comparable to the other datasets. Shading in a lighter color is added to show the standard deviation of the results; when uncertainty is small due in part to a large number of data points, shading area may not show up.

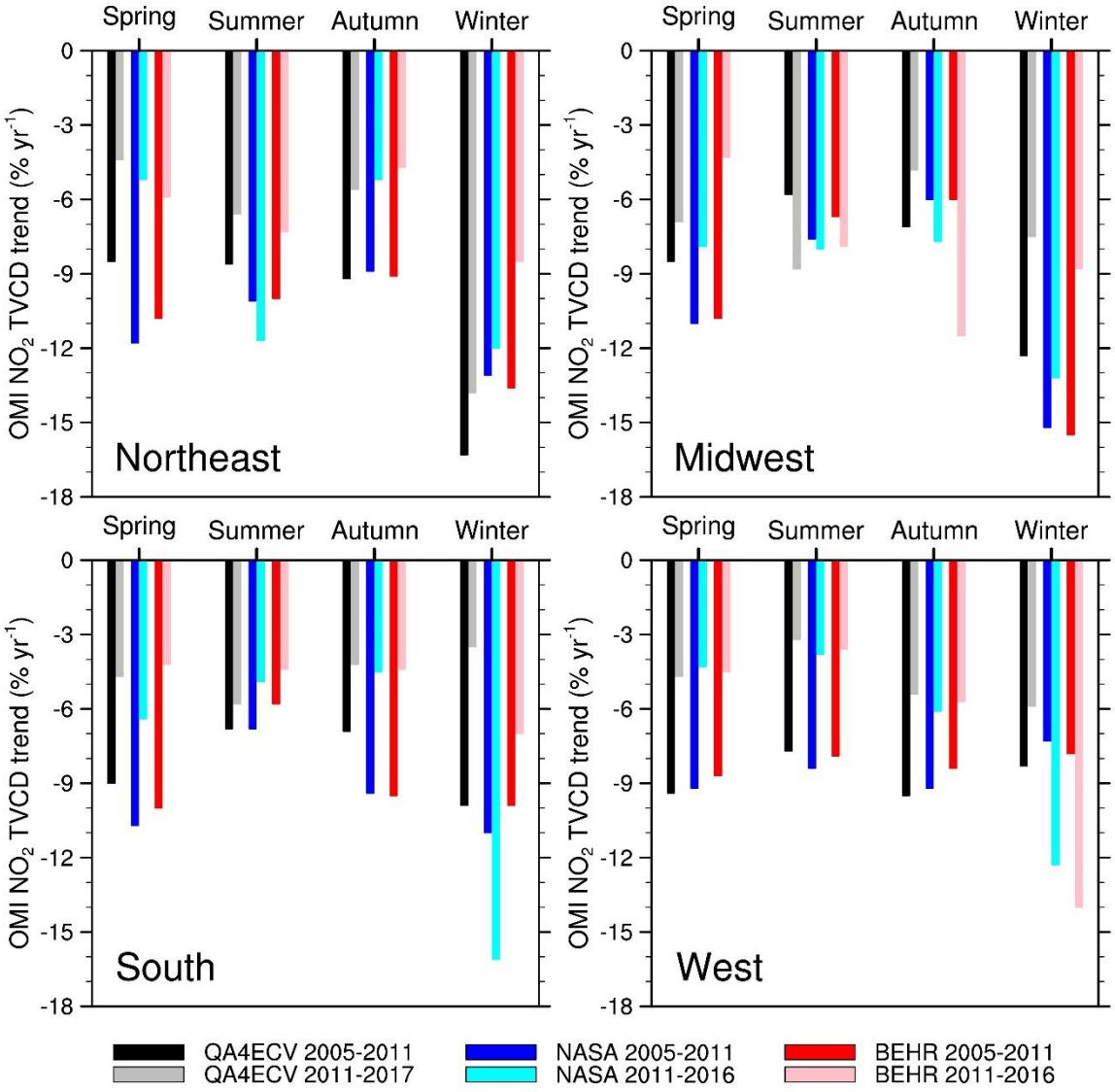


728
729 Figure 7. Pre- and post-2011 OMI $NO_2$ TVCD trends for 4 seasons in the urban regions of
730 Northeast, Midwest, South, and West. Black bars denote OMI-QA4ECV $NO_2$ TVCD trends from
731 2005 – 2011; gray bars denote the corresponding trends during 2011 – 2017. Blue bars denote
732 OMI-NASA trends from 2005 – 2011; cyan bars denote NASA-OMI trends from 2011 – 2016.
733 Red bars denote BEHR-OMI trends from 2005 – 2011; pink bars denote OMI-BEHR trends from
734 2011 – 2016.

735